Chapter 6

Magnetoresistance and Structural Characterization of Electrospun $La_{1-x}Sr_xMnO_3$ Nanowire Networks

Xian Lin Zeng, Thomas Karwoth,
Anjela Koblischka-Veneva, Michael R. Koblischka,
Jörg Schmauch, Uwe Hartmann and Thomas Hauet

Additional information is available at the end of the chapter

http://dx.doi.org/10.5772/intechopen.80451

Abstract

Nanowire network fabrics of $La_{1-x}Sr_xMnO_3$ (LSMO) with different doping levels x = 0.2, 0.3, and 0.4 were fabricated by means of electrospinning. The resulting nanowires are up to 100 μm long with a mean diameter of about 230 nm. The nanowires form a nonwoven fabric-like arrangement, allowing to attach electric contacts for magnetoresistance (MR) measurements. The resistance in applied magnetic fields and the MR effect were measured in the temperature range 2 K < T < 300 K in magnetic fields up to 10 T applied perpendicular to the sample surface. An MR ratio of about 70% is obtained for x = 0.2 at 10 T applied field and T = 20 Kr. The highest low-field MR of 5.2% (0.1 T) is obtained for the sample with x = 0.2. Magnetization measurements reveal the soft magnetic character of the samples. A thorough analysis of the microstructure of these nanowire networks is performed including scanning electron microscopy (SEM) and transmission electron microscopy (TEM).

Keywords: LSMO, electrospinning, nanowires, magnetoresistance, microstructure

1. Introduction

Colossal magnetoresistance (CMR) is a property of some materials, mostly manganese-based perovskite oxides that enables them to dramatically change their electrical resistance in the presence of a magnetic field, i.e., magnetoresistance (MR) [1–3]. To bring the CMR materials toward applications, it is still necessary to further optimize the sample processing to find the optimal microstructure, especially concerning grains in the nanometer range. The low-field

magnetoresistance response (LFMR) of such manganese perovskite oxides like $La_{1-x}Sr_xMnO_3$ (LSMO) with different doping levels x is closely connected to the existence of interfaces and grain boundaries (GBs) within the samples [4–7], and the high-field magnetoresistance (HFMR) was found to increase progressively on decreasing the grain size [8]. Therefore, the measurements of nanostructured or nano-sized samples are an important issue to provide a deeper understanding and further improvement of the MR effect, especially for the improvement of the behavior of devices based on the MR effect in reduced dimensions.

Commonly, the manganese perovskite samples studied in the literature are prepared as bulks or as thin films, mainly on $SrTiO_3$ substrates. Nanometer-sized bridges are then prepared using lithography techniques or the focused ion-beam technique [9, 10]. The use of a substrate in the case of thin-film samples is always causing strain effects within the functional layer due to the lattice mismatch, which may play an important influence on the resulting magnetic properties [11]. The situation may be considerably different in nanostructures without substrate, being recently investigated in several types of nanoscale composites [12–14]. These nanostructures include nanorods, nanowires, nanotubes, and nanobelts; all of them having specific physical properties depending on the chosen preparation route.

In the present contribution, we have fabricated nanowire network fabrics of $La_{1-x}Sr_xMnO_3$ (LSMO) with different doping levels x by means of the electrospinning technique [15–17]. This technique is common for the fabrication of organic polymer nanostructures but can be modified by employing different precursors to deliver inorganic compounds. Up to now, only a small number of reports are dealing with magnetic nanostructures prepared in this way [17–19]. In the case of LSMO, exhibiting the CMR effect, the resulting nanowires are of polycrystalline nature with a high-aspect ratio (length up to 100 μm and diameters of about 230 nm) and show a large number of grain boundaries (GBs) within each individual nanowire. In Ref. [19], individual nanowires were separated from the as-spun networks and placed on a prepatterned substrate. Electric contacts were prepared using Ti/Cu electrodes, and the nanowires could be measured individually, allowing to observe a dependence of the MR on the nanowire diameter. Single nanowires of CMR materials may be employed as sensitive gas sensor elements or electrodes [20–22].

However, the as-spun nanowires form a nonwoven fabric-like network, where numerous interconnects between the individual nanowires are formed in the final heat treatment step. As a result, the current flow through such a nanowire network fabric shows percolative character, and several sub-loops can be formed. The interconnects between the individual nanowires add additional crossover points for the currents and can enhance the tunneling transport across the interfaces, together with the GBs. This additional scattering of the electrons at the interfaces provided by the interconnects is lost when measuring only extracted parts of the nanowires as done in Ref. [19]. Furthermore, no information on the LSMO grain size of their nanowires was presented. An analysis of the grain sizes within our nanowires showed values ranging between 10 and 32 nm. Therefore, it is obvious that the LSMO grains within the present nanowires are smaller as compared to, e.g., Ref. [8].

Therefore, we may expect interesting new properties of this new class of magnetic material. Furthermore, the nanowire network fabrics are an extremely lightweight material with a

http://dx.doi.org/10.5772/intechopen.80451

density of about 0.084 g/cm^3, which is considerably less than the theoretical density of 6.5 g/cm^3 [23]. Furthermore, there is no sample size limitation imposed by the fabrication technique, as electrospinning may produce very large sample sizes [24]. This makes such fabrics interesting for applications in bulk form, whenever the weight of the sample counts.

In order to achieve a better understanding of the transport properties through these nanowire network fabrics, we also performed a thorough microstructure analysis including scanning electron microscopy (SEM) and transmission electron microscopy (TEM).

2. Experimental procedures

The electrospinning precursor is prepared by dissolving La, Sr, and Mn acetates in PVA (high-molecular-weight polyvinyl alcohol). The PVA is slowly added to the acetate solution with a mass ratio of 2.5:1.5. This solution is stirred at 80°C for 2 h and then spun into cohering nanofibers by electrospinning. To remove the organic compounds and to form the desired LSMO phase, the sample is subsequently heat treated in a lab furnace. An additional oxygenation process is required to obtain the correct phase composition. The constituent phase was checked by means of X-ray diffraction (XRD) and EDX analysis. Further details about the electrospinning process of ferromagnetic and superconducting nanowires are given elsewhere [25–28].

Figure 1. Images of the electrospun samples fabricated from the $La_{0.8}Sr_{0.2}MnO_3$ precursor. Images (a) and (b) present a view of an as-prepared sample before thermal treatment, whereas images (c) and (d) give a $La_{0.8}Sr_{0.2}MnO_3$ sample after the whole annealing process applied. As can be directly seen from the images, the size (area) of the sample shrinks to one sixth as compared to the original one after the thermal treatment.

Figure 1(**a**, **b**) presents photographs of an as-grown $La_{0.8}Sr_{0.2}MnO_3$ nanowire fabric. The nanowire fabric consists of polymer nanowires containing the ceramic precursor material. The as-grown fabric has a white color, and the entire fabric sample is fully flexible. **Figure 1**(**c**, **d**) finally presents the fully reacted sample after having received the full thermal treatment. The reacted sample shows a fully black color, indicating the completed chemical reaction. As a result, the final nanowire network fabric is extremely thin and brittle. Here, it is important to note that the sample size shrunk to about one sixth of its original size. This shrinkage has to be considered for the application of such fabric-like materials. In the thermal treatment, numerous interconnects between the individual nanowires are formed, which are essential for the resulting current flow through the sample.

The entire nanowire network was electrically connected by means of silver paint and Cu wires (50 μm diameter) to the sample holder. Due to the high fragility of the ceramic sheet, a pseudo four-point configuration is realized where the current and voltage links connect immediately on the sample contacts. This arrangement is presented in **Figure 2**. The magnetoresistance is measured in a 10/12 T bath cryostat (Oxford Instruments Teslatron) with a Keithley source meter (model 2400) as a current source, and the voltage is recorded using a Keithley 2001 voltmeter.

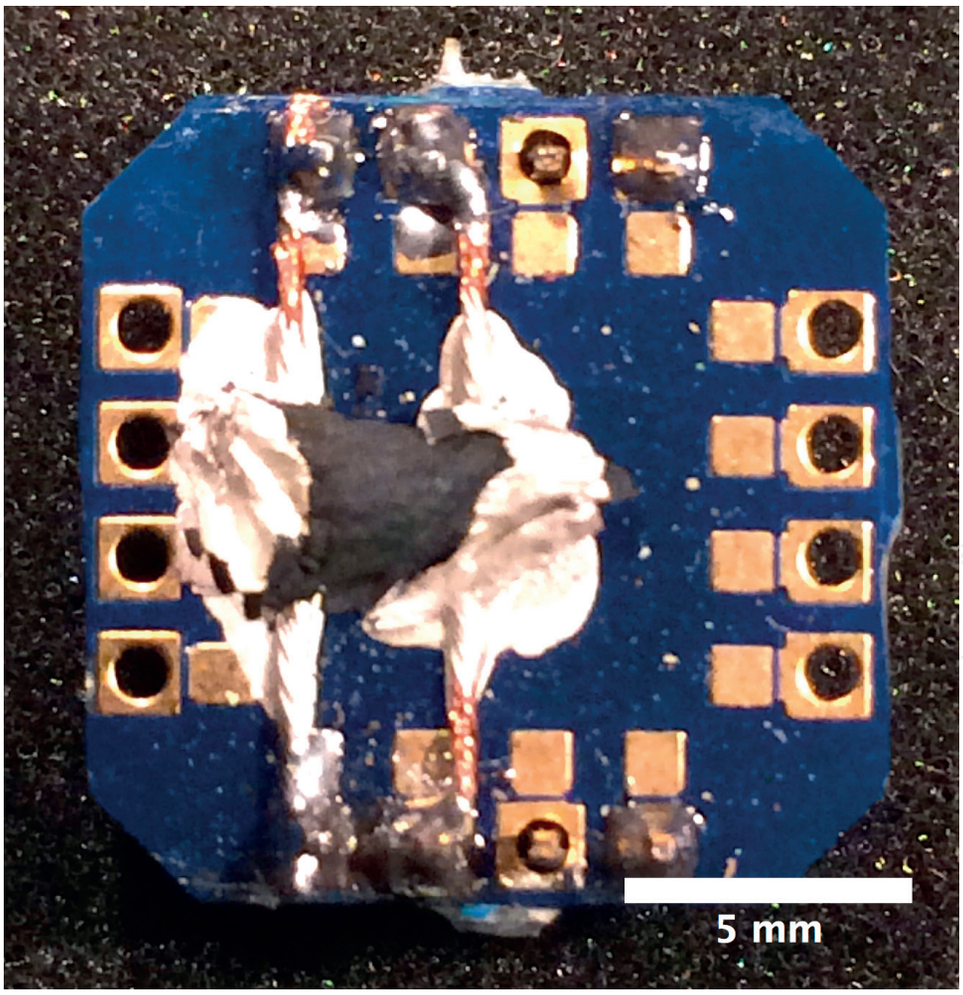

Figure 2. Nanowire network sample with electrical contacts for the quasi four-point measurement.

http://dx.doi.org/10.5772/intechopen.80451

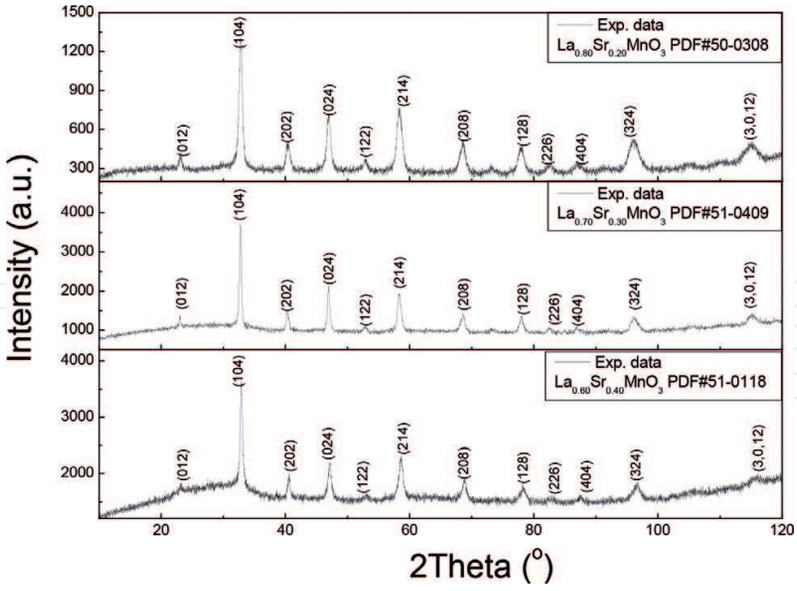

Figure 3. XRD measurements on all three types of LSMO nanowire fabric samples.

The constituent phases of the samples were determined by means of a high-resolution automated RINT2200 X-ray powder diffractometer using Cu-K^{α} radiation (40 kV, 40 mA) **Figure 3**. SEM imaging was performed using a Hitachi S800 scanning electron microscope operating at a voltage of 10 kV, and the TEM analysis was performed by a JEOL JSM-7000F transmission electron microscope (200 kV, LaB_6 cathode). For TEM imaging, pieces of the nanowire network fabrics were deposited on carbon-coated TEM grids. High-resolution TEM and EBSD were performed on selected nanowire sections being thin enough for electron transmission (**Figure 6**).

The magnetization of the nanowire networks was measured using a SQUID magnetometer (Quantum Design MPMS3) with ±7 T magnetic field applied perpendicular to the sample surface, using a piece of the nanowire network fabric with a size of 14.86 mm^2.

3. Results and discussion

3.1. Microstructure

Scanning electron microscopy revealed an average diameter of the resulting nanowires of around 220 nm and a length of more than 100 μm. Fabric-like nanowire networks with numerous interconnects are formed after the heat treatment. The individual nanowires are polycrystalline with a grain size of about 10–30 nm, which corresponds to the dimensions obtained via transmission electron microscopy and electron backscatter diffraction (EBSD) analysis.

This is presented in **Figure 4** giving SEM images of the nanowire network fabrics at 5000× magnification (first column) and at higher magnification (10,000×, second column) for all LSMO samples studied here. **Figure 4(a)** and **(b)** shows the sample x = 0.2, (c) and (d) the

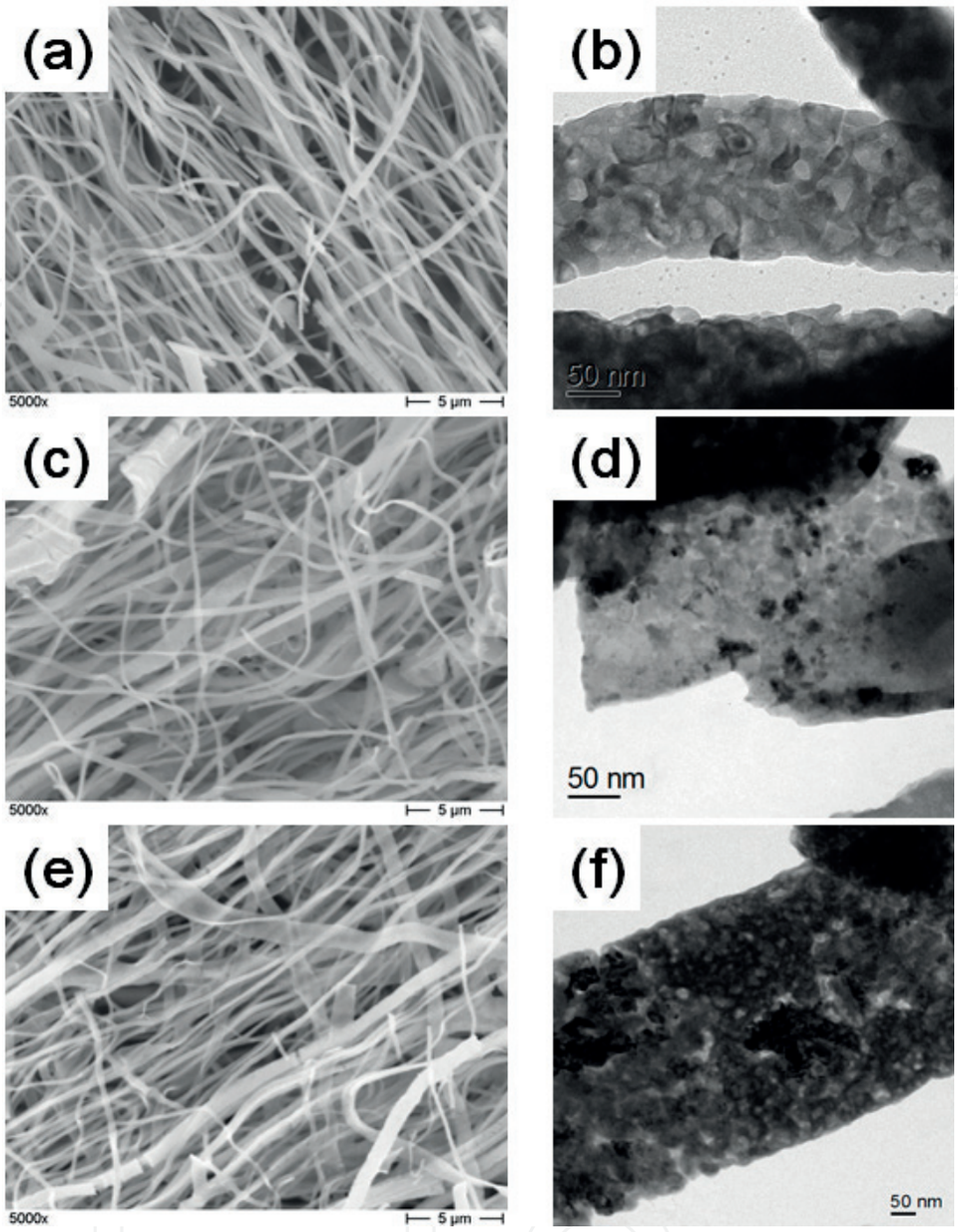

Figure 4. SEM images of the nanowire network fabrics at 5000× magnification (first column) and at higher magnification (10,000×, second column) for all LSMO samples studied here. Images (a) and (b) show the sample $x = 0.2$, (c) and (d) the sample $x = 0.3$, and (e) and (f) the sample $x = 0.4$. The low-magnification images (a, c, and e) present the individual nanowires forming the network fabrics and the numerous interconnects between them. The images with higher resolution (b, d, and f) reveal the polycrystalline structure of the LSMO nanowires. Several small LSMO grains form stacks building up a nanowire.

sample $x = 0.3$, and (e) and (f) the sample $x = 0.4$. The low-magnification images (a, c, and e) present the individual nanowires forming the network fabrics and the numerous interconnects between them. These interconnects, formed during the final heat treatment step, are essential for the current flow through the entire sample perimeter and provide additional scattering at their interfaces. The images with higher resolution (b, d, and f) reveal the polycrystalline structure of the LSMO nanowires. Several small LSMO grains form stacks building up a

http://dx.doi.org/10.5772/intechopen.80451

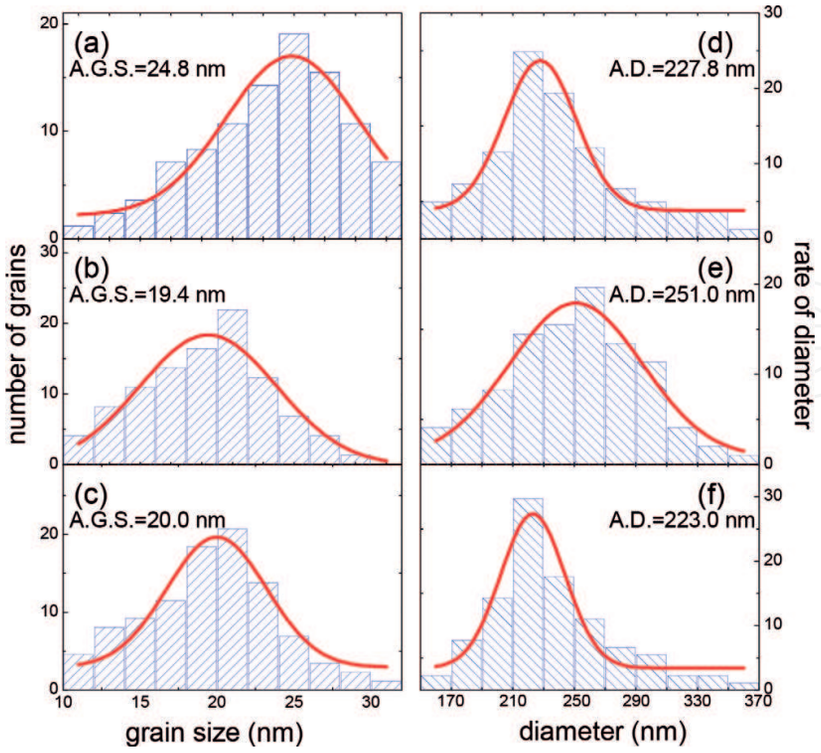

Figure 5. Statistics of the nanowire average grain size (AGS) and the diameter (AD): (a) and (d) $La_{0.8}Sr_{0.2}MnO_3$, (b) and (e) $La_{0.7}Sr_{0.3}MnO_3$, and (c) and (f) $La_{0.6}Sr_{0.4}MnO_3$.

nanowire. Furthermore, it is obvious from these images that the LSMO grains do not show a texture but are randomly oriented with high-angle grain boundaries between them.

Figure 5 presents the detailed analysis of the nanowire diameters and the LSMO grain size determined from several SEM and TEM images. Graphs (a), (b), and (c) show the grain size analysis. The average values were determined using a Gauss fit to the data (indicated by a red line). For the sample $x = 0.2$, the grain size determined from TEM images varies between 10 and 32 nm with an average of 24.8 nm. Sample $x = 0.3$ shows grain sizes ranging between 10 and 30 nm with an average of 19.4 nm, and sample $x = 0.4$ shows an equal distribution of grain sizes with an average grain size of 20 nm. For all samples, the grain sizes determined from the TEM images are larger than the average grain size estimated from XRD, indicating that there are multiply connected domains in the sample. On the sample $x = 0.2$, we also performed an EBSD analysis of the grain orientations [29], demonstrating the presence of a large number of high-angle grain boundaries within an individual nanowire. The graphs of the nanowire diameters (d, e, f) reveal an average diameter of 227.8 nm for the sample $x = 0.2$, 251.0 nm for sample $x = 0.3$, and 223.0 nm for sample $x = 0.4$. Note that also here the sample $x = 0.4$ exhibits a much narrower size spectrum as compared to the other samples studied here.

Figure 6 shows finally some high-resolution TEM images of all three LSMO samples studied here. **Figure 6(a)** and **(b)** gives grains and their grain boundaries of sample $x = 0.2$, (c) and (d) images with the same magnification of sample $x = 0.3$, and (e) and (f) those of sample $x = 0.4$. For all samples, the LSMO grain size is around 20 nm, and the grains are randomly oriented, resulting in the presence of high-angle grain boundaries between the grains. Furthermore,

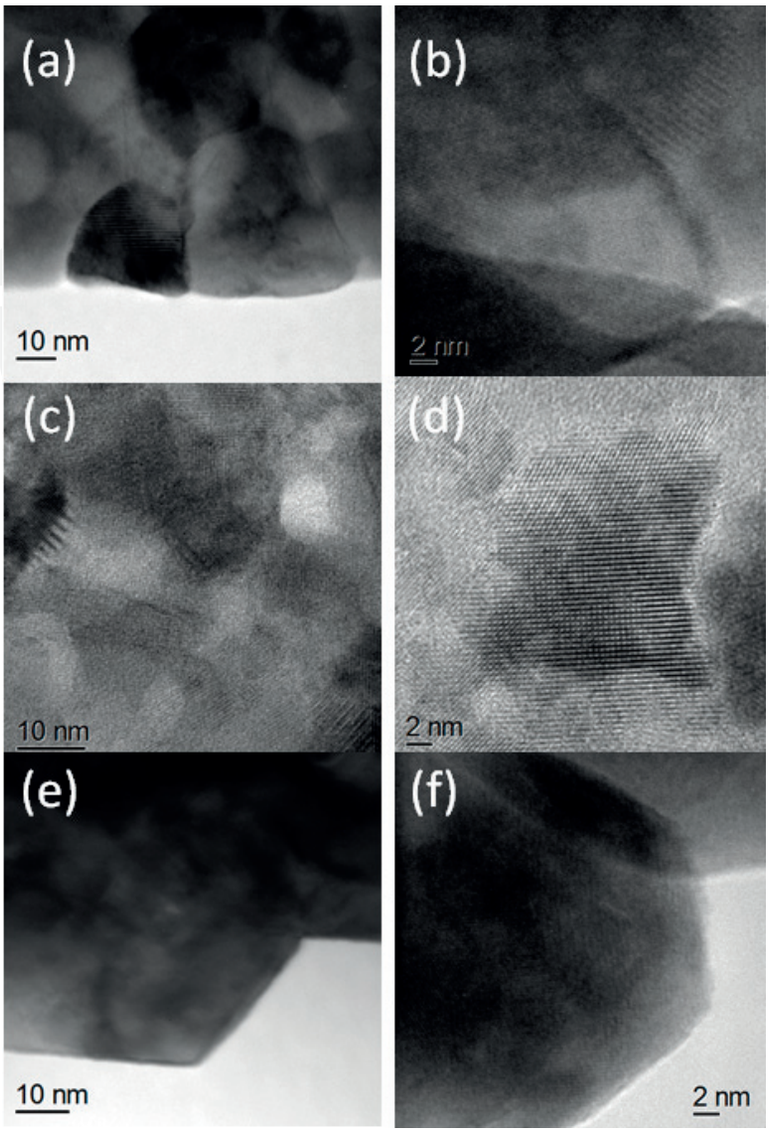

Figure 6. High-resolution TEM images with two magnifications of all three types of samples studied here. (a, b) sample $x = 0.2$, (c, d) sample $x = 0.3$, and (e, f) sample $x = 0.4$. The LSMO grains of all samples have sizes of ~20 nm, and the grains are randomly oriented with high-angle grain boundaries between them.

some grain clusters connected with low-angle grain boundaries are also visible, which explains the differences between the grain sizes determined from X-ray data and from TEM images and EBSD [29]. The nanowires are built up from stacks of several individual LSMO grains.

3.2. Magnetization data

Figure 7 presents the magnetization data obtained for all three compositions. The soft magnetic character of the LSMO fabric samples is clearly revealed. From the Sr-doping level $x = 0.2$ to $x = 0.4$, the saturation magnetization (M_s) is at 10 K 52.12, 58.13, 55.03 emu/g, and at 300 K, and the results are 18.10, 33.09, and 24.62 emu/g, respectively. These values are lower than the ones from the corresponding bulk materials (56 emu/g [30], 33.09 emu/g [31], 24.62 emu/g [32]). The $x = 0.3$ sample shows the highest M_s among the three compositions, while the $x = 0.2$ sample shows the lowest ones at both 10 and 300 K. This matches the conclusion drawn from

http://dx.doi.org/10.5772/intechopen.80451

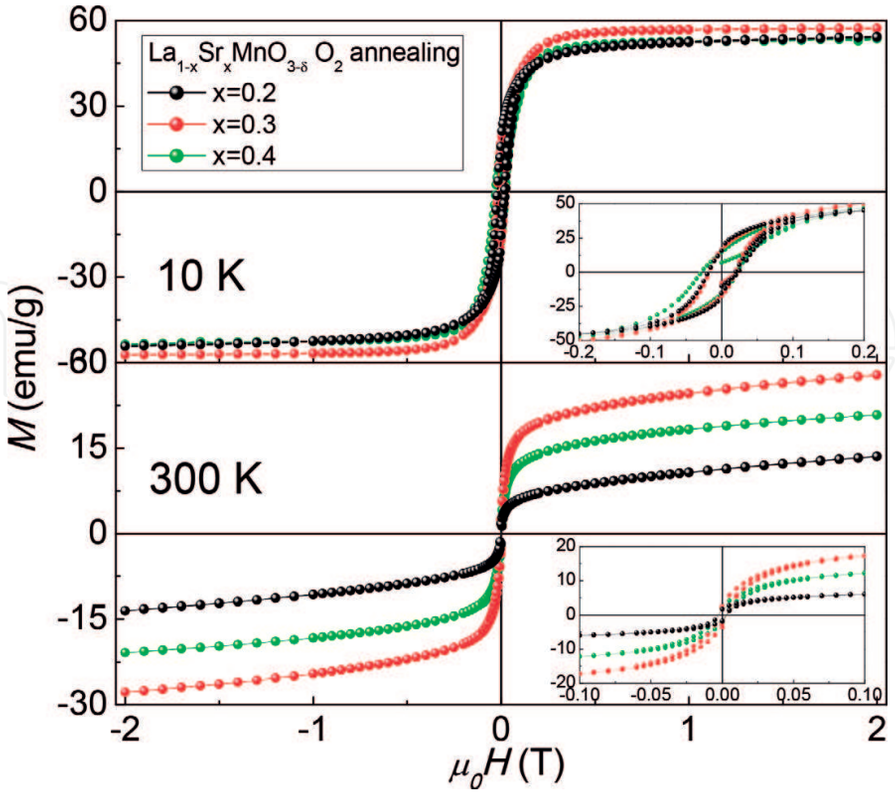

Figure 7. $M(H)$ measurement of the LSMO nanowires at T = 10 and 300 K for the LSMO nanowire network fabrics with x = 0.2, 0.3, and 0.4. The insets present the low-field part of the $M(H)$ loops.

bulk materials that the optimized doping level around x = 0.33 supplies the strongest magnetism. The M_s value of all our samples being lower than the bulk values can be attributed to the smaller LSMO grain size of our nanowire network fabric samples.

3.3. MR data

With respect to the literature, the MR data can be divided into two different regimes. According to Ref. [8], the high-field magnetoresistance (HFMR) behavior sheds light on the influence of the sample microstructure via the interface response. Therefore, analyses of the electronic transportation properties and of the magnetoresistive effects of the nanowire networks were carried out by four-probe measurements in external magnetic fields up to 10 T. Firstly, we have a look at the high-field regime. **Figure 8** presents the resistance measurements for the samples x = 0.2, 0.3, and 0.4 with the temperature swept from 5 to 300 K. The magnetic field is applied perpendicular to the surface of the nanowire network, i.e., the current flow is mainly perpendicular to the applied field. Magnetoresistance plots are calculated from the data obtained by these sweep measurements at different field strengths using the relation

$$\mathrm{MR}[\%] = \frac{R_H(T) - R_0(T)}{R_0(T)}. \tag{1}$$

As result, we find a maximum MR for the sample x = 0.2 at low temperatures and 10 T applied magnetic field of 70%.

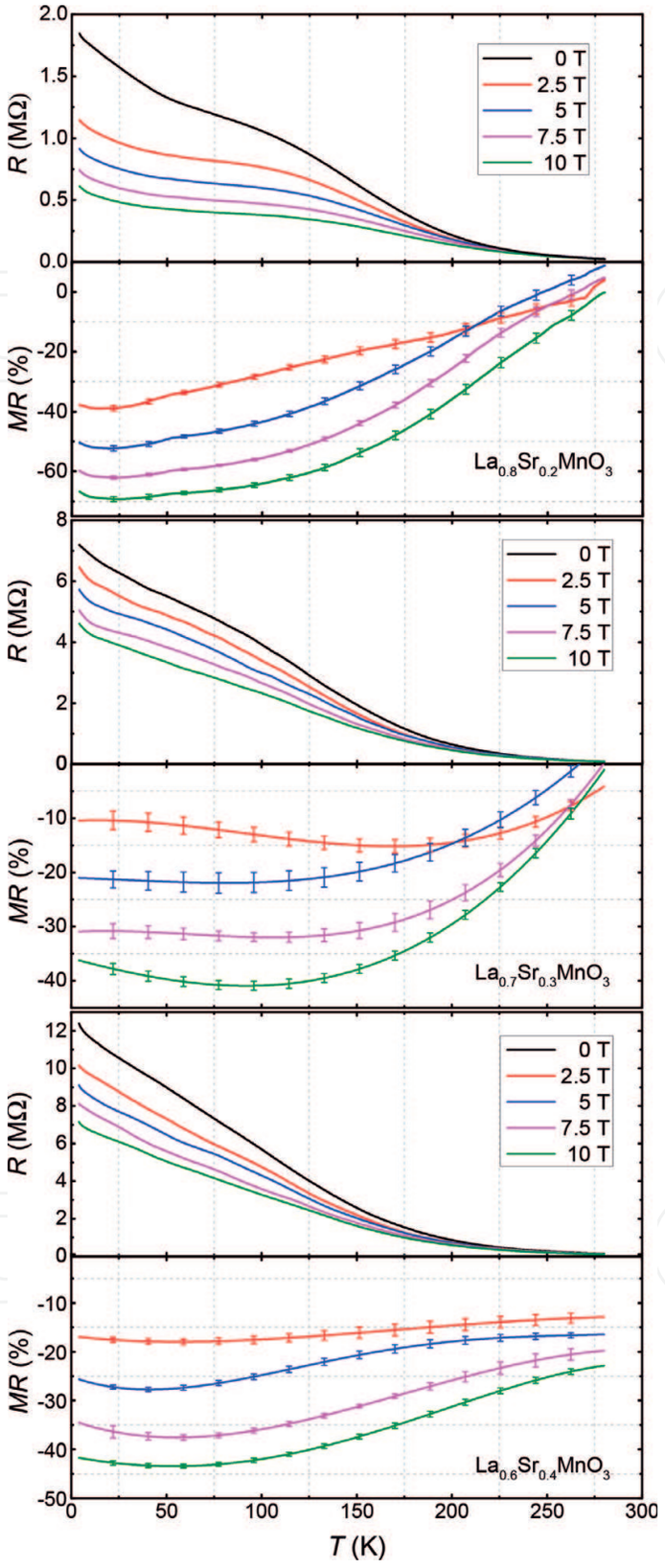

Figure 8. Resistance and MR ratio of all LSMO samples measured up to 10 T applied magnetic field ($H \perp$sample surface) in the range 2 K < T < 275 K: (a) x = 0.2, (b) x = 0.3, and (c) x = 0.4.

http://dx.doi.org/10.5772/intechopen.80451

Doping level	MR(%) at 1 T		
x	100 K	270 K	MR max.
0.2	10.24	130	20.66 (22 K)
0.3	6.23	5.98	14.54 (203 K)
0.4	23.58	7.69	26.01 (63 K)
	MR(%) at 2.5 T		
0.2	27.69	1.81	39 (14 K)
0.3	13.2	6.32	15.18 (169 K)
0.4	17.48	13.00	17.97 (57 K)
	MR(%) at 10 T		
0.2	64.12	4.62	69.28 (25 K)
0.3	40.88	5.84	40.93 (92 K)
0.4	41.99	23.47	43.45 (54 K)

The last row gives the maximum MR obtained, together with the respective temperature.

Table 1. MR comparison of all LSMO samples measured here at 1, 2.5, and 10 T applied magnetic field.

Table 1 summarizes our findings at three selected magnetic fields for the three doping levels studied here, and the last row of **Table 1** gives the maximum MR obtained, together with the respective temperature.

At 100 K, sample $x = 0.4$ shows the highest MR of 23.58% (close to the overall maximum of 26%) at 1 T applied field. In higher applied fields, the maximum value of the MR shifts to sample $x = 0.2$. A maximum MR ratio of 26.01 at an applied field of 1 T (63 K) is obtained for the sample $x = 0.4$. At 2.5 T applied field, the maximum MR of 17.97 (57 K) is found in sample $x = 0.4$.

At 10 T applied magnetic field, the maximum MR rate of 69.28% (25 K) is found in sample $x = 0.2$. Note also that the highest MR of sample $x = 0.3$ is obtained at a relatively high temperature, ranging from 203 K (1 T) to 92 K (10 T). Secondly, **Figure 9** shows the MR ratio of sample $x = 0.2$ as a function of applied field for various temperatures. The MR is found to increase on lowering the temperature down to 50 K, whereas the MR at low temperature (3 K) is found to be smaller as compared to the 50 K data. The inset of **Figure 9** presents the LFMR at an applied magnetic field of 0.1 T for the sample $x = 0.2$, showing a maximum LFMR of 5.2% at $T = 50$ K.

3.4. Discussion

From the graphs and the tables presented here, three main features can be deduced: Firstly, there is a suppression of the metal-insulator transition. This provides another evidence of the size effect. Nanoscale grains are always accompanied by a large number of grain boundaries, which enhance electron scattering. The metallic behavior is negatively influenced by the Coulomb blockade [13], and as a result, an upturn of the resistivity appears at low temperatures. On the

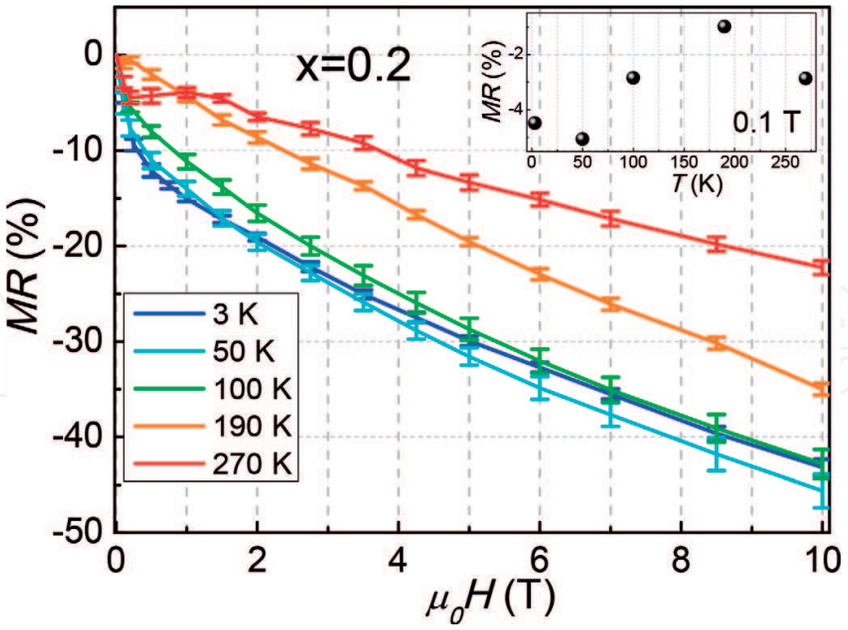

Figure 9. Magnetoresistance of $La_{0.8}Sr_{0.2}MnO_3$ nanowires as function of the applied field for various temperatures. The inset gives the LFMR at 0.1 T applied magnetic field.

other hand, the influence from certain size effects varies with the doping level. So, a step-shape resistance behavior can be observed for the x = 0.2 sample, which indicates that the metal-insulator transition is not completely suppressed. However, in the x = 0.4 sample, the resistance decreases almost linearly from 5 K to 200 K. Secondly, the x = 0.3 sample with the highest saturation magnetization shows the weakest MR effect, and inversely, the x = 0.2 sample exhibits the strongest MR effect at low temperatures. At 2.5 T, the maximum of the MR is already over 40%, which points to an obvious LFMR effect. The increase of the MR with reducing magnetization has been reported by Balcells et al. [8]. In their work, the variation of the grain size is the main reason of the behavior observed. In contrast to this, there is no obvious grain size difference between our samples. The dependence of the MR on the magnetization requires further investigation. Thirdly, at around 200 K with the doping level x = 0.2 and 0.3, the MR curves at 2.5 T have a crossover with the curves at other fields, which means that above 200 K, the absolute value of the magnetoresistance does not monotonously increase with the external field.

To enable a comparison with data on other LSMO sample types but with the same chemical composition (x = 0.2) published in the literature, we summarize some data at 1 T applied magnetic field in **Table 2** and compare them with our results.

From **Table 2**, we see that the nanowire sample x = 0.2 exhibits a larger MR of 20.66% as compared to the nanoparticles and the powder samples of the same chemical composition studied in the literature, however, at some lower temperature. This points clearly to the important contribution of the much smaller LSMO grains in our nanowire network fabric samples, and the additional scattering at the numerous interconnects provides extra MR.

Jugdersuren et al. [19] reported a large LFMR at room temperature in their LSMO nanowires extracted from the networks produced by electrospinning and showed a dependence of the

$La_{0.8}Sr_{0.2}MnO_3$	MR(%) at 1 T		
Type	100 K	270 K	MR max
Nanowires [33]	11.2	3.93	20.66 (22 K)
Nanoparticles [34]	19.36	4.66	18.7 (79 K)
Powder [35]	13.56	6.47	17.66 (50 K)

Table 2. Magnetoresistance (MR) comparison of different sample types (nanowires, nanoparticles, and powder) of $La_{0.8}Sr_{0.2}MnO_3$ samples studied in the literature at 1 T applied magnetic field.

LFMR on the nanowire diameter, but no information on the LSMO grain size was presented. However, the LFMR at 300 K for our sample is comparable to their data, even though the chemical composition is somewhat different. Nevertheless, this demonstrates that the LFMR as well as the HFMR can be considerably enhanced by reducing the nanowire diameter as well as the LSMO grain size.

4. Conclusion

Nonwoven nanowire networks of LSMO with three doping levels x = 0.2, 0.3, and 0.4 were fabricated by means of electrospinning. The magnetoresistance effect of these nanowire fabrics was measured up to 10 T applied field between 5 K and 300 K. The reduced dimensions of the nanowires and the large number of interconnects between them were found to increase the MR effect as compared to bulk samples. An MR ratio of 70% was observed for the sample x = 0.2 at low temperatures and 10 T applied magnetic field.

Acknowledgements

We thank Prof. V. Presser (Saarland University and Institute of New Materials, Saarbrücken) for giving us the possibility to use the electrospinning apparatus. The collaboration Saarbrücken-Nancy was supported by the EU-INTERREG IVa project "GRMN." This work is supported by Volkswagen Foundation and DFG project Ko 2323/8, which is gratefully acknowledged.

Author details

Xian Lin Zeng[1], Thomas Karwoth[1], Anjela Koblischka-Veneva[1], Michael R. Koblischka[1]*, Jörg Schmauch[1], Uwe Hartmann[1] and Thomas Hauet[2]

*Address all correspondence to: m.koblischka@gmail.com

1 Institute of Experimental Physics, Saarland University, Saarbrücken, Germany

2 Institut Jean Lamour, UMR CNRS-Université de Lorraine, Vandœvre-lès-Nancy, France

References

[1] Jin S, Tiefel TH, McCormack M, Fastnacht RA, Ramesh R, Chen LH. Thousandfold change in resistivity in magnetoresistive La-Ca-Mn-O films. Science. 1994;**264**:413-415

[2] Rodriguez LM, Attfield JP. Cation disorder and size effects in magnetoresistive manganese oxide perovskites. Physical Review B. 1996;**54**:R15622-R15625

[3] Ramirez AP. Colossal magnetoresistance. Journal of Physics: Condensed Matter. 1997;**9**: 8171-8199

[4] Hwang HY, Cheong S-W, Ong NP, Batlogg P. Spin-polarized intergrain tunneling in $La_{2/3}Sr_{1/3}MnO_3$. Physical Review Letters. 1996;**77**:2041

[5] Mahesh R, Mahendiran R, Raychaudhuri AK, Rao CNR. Effect of particle size on the giant magnetoresistance of $La_{0.7}Ca_{0.3}MnO_3$. Applied Physics Letters. 1996;**68**:2291

[6] Li XW, Gupta A, Xiao G, Gong GQ. Low-field magnetoresistive properties of polycrystalline and epitaxial perovskite manganite films. Applied Physics Letters. 1997;**71**:1124

[7] Kar S, Sarkar J, Ghosh B, Raychaudhuri AK. Effect of grain boundaries on the local electronic transport in nanostructured films of colossal magnetoresistive manganites. The Journal of Nanoscience and Nanotechnology. 2007;**7**:2051

[8] Balcells L, Fontcuberta J, Martinez B, Obradors X. High field magnetoresistance at interfaces in manganese perovskites. Physical Review B. 1998;**58**:R14697

[9] Liu D, Liu W. Room temperature ultrahigh magnetoresistance nanostructure ($La_{2/3}Sr_{1/3}$) MnO_3 films growth on $SrTiO_3$ substrate. Ceramics International. 2012;**38**:2579

[10] Marin L, MorelloÌ L, Algarabel PA, Rodiguez LA, Magen C, De Teresa JM, et al. Enhanced magnetotransport in nanopatterned manganite nanowires. Nano Letters. 2012;**11**:103

[11] Hwang HY, Iwasa Y, Kawasaki M, Keimer B, Nagaosa N, Tokura Y. Emergent phenomena at oxide interfaces. Nature Materials. 2014;**14**:423

[12] Li L, Liang L, Wu H, Zhu X. One-dimensional perovskite manganite oxide nanostructures: Recent developments in synthesis, characterization, transport properties, and applications. Nanoscale Research Letters. 2016;**11**:121

[13] Sarkar T, Kamalakar MV, Raychaudhuri AK. Electrical transport properties of nanostructured ferromagnetic perovskite oxides $La_{0.67}Ca_{0.33}MnO_3$ and $La_{0.5}Sr_{0.5}CoO_3$ at low temperatures (5 K 0.3 K) and high magnetic field. New Journal of Physics. 2012;**14**:033026

[14] Dwivedi GP, Kumar M, Shahi P, Barman A, Chatterjee S, Ghosh AK. Low temperature magnetic and transport properties of LSMO-PZT nanocomposites. RSC Advances. 2015;**5**: 30748

[15] Li D, McCann JT, Xia YN. Electrospinning: A simple and versatile technique for producing ceramic nanofibers and nanotubes. Journal of the American Ceramic Society. 2006;**89**:1861

[16] Wu H, Pan W, Lin D, Li H. Electrospinning of ceramic nanofibers: Fabrication, assembly and applications. Journal of Advanced Ceramics. 2012;**1**:2

[17] Li D, Herricks T, Xia YN. Magnetic nanofibers of nickel ferrite prepared by electrospinning. Applied Physics Letters. 2003;**83**:4586

[18] Yensano R, Pinitsoontorn S, Amornkitbamrung V, Maensiri S. Fabrication and magnetic properties of electrospun $La_{0.7}Sr_{0.3}MnO_3$ nanostructures. Journal of Superconductivity and Novel Magnetism. 2014;**27**:1553

[19] Jugdersuren B, Kang S, DiPietro RS, Heiman D, McKeown D, Pegg IL, et al. Large low field magnetoresistance in $La_{0.67}Sr_{0.33}MnO_3$ nanowire devices. Journal of Applied Physics. 2011;**109**:016109

[20] Liu Y, Sun X, Li B, Lei Y. Tunable p-n transition behaviour of a p-$La_{0.67}Sr_{0.33}MnO_3$/n-CeO_2 nanofibers heterojunction for the development of selective high temperature propane sensors. Journal of Materials Chemistry A. 2014;**2**:11651

[21] Xu D, Luo L, Ding Y, Xu P. Sensitive electrochemical detection of glucose based on electrospun $La_{0.88}Sr_{0.12}MnO_3$ nanofibers modified electrode. Analytical Biochemistry. 2015; **489**:38

[22] Zhi M, Koneru A, Yang F, Manivannan A, Li J, Wu N. Electrospun $La_{0.8}Sr_{0.2}MnO_3$ nanofibers for a high-temperature electrochemical carbon monoxide sensor. Nanotechnology. 2012;**23**:305501

[23] Armstrong TJ, Virkar AV. Performance of solid oxide fuel cells with LSGM-LSM composite cathodes. Journal of the Electrochemical Society. 2002;**149**(12):A1565-A1571

[24] Huang ZM, Zhang YZ, Kotaki M, Ramakrishna S. A review on polymer nanofibers by electrospinning and their application in nanocomposites. Composites Science and Technology. 2003;**63**:2223-2253

[25] Zeng XL, Koblischka MR, Hartmann U. Synthesis and characterization of electrospun superconducting (La,Sr)CuO_4 nanowires and nanoribbons. Materials Research Express. 2015;**2**:095022

[26] Koblischka MR, Zeng XL, Karwoth T, Hauet T, Hartmann U. Transport and magnetic measurements on Bi-2212 nanowire networks prepared via electrospinning. IEEE Transactions on Applied Superconductivity. 2016;**26**:1800605

[27] Zeng XL, Koblischka MR, Karwoth T, Hauet T, Hartmann U. Preparation of granular Bi-2212 nanowires by electrospinning. Superconductor Science and Technology. 2017;**30**:035014

[28] Koblischka MR, Zeng XL, Laurent F, Karwoth T, Koblischka-Veneva A, Hartmann U, et al. Characterization of electrospun BSCCO nanowires with reduced preparation temperature. IEEE Transactions on Applied Superconductivity. 2018;**28**:7200505

[29] Koblischka-Veneva A, Koblischka MR, Zeng XL, Schmauch J. Journal of Magnetism and Magnetic Materials. submitted for publication

[30] Dominiczak M, Ruyter A, Limelette P, Laffez IM, Giovannelli F, Rossell MD, et al. Effects of nanocracks on the magnetic and electrical properties of $La_{0.8}Sr_{0.2}MnO_3$ single crystals. Solid State Communications. 2009;**149**:1543

[31] Huang BX, Liu YH, Yuan XB, Wang CJ, Zhang RZ, Mei LM. The unusual magneto-transport properties of $La_{0.67}Sr_{0.33}MnO_3$ with Nb_2O_5 addition. Journal of Magnetism and Magnetic Materials. 2004;**280**:176

[32] Vijayanandhini K, Kutty TRN. Magnetically tuneable nonlinear electronic properties of ZnO/La(Sr)MnO_3 composites. Journal of Physics D: Applied Physics. 2006;**39**:2902

[33] Karwoth T, Zeng XL, Koblischka MR, Hartmann U, Chang C, Hauet T, et al. Magnetoresistance and structural characterization of electrospun $La_{1-x}Sr_xMnO_3$ nanowire networks. Solid State Communications. submitted for publication

[34] Nagabhuhana BM, Sreekanth Chakradhar RP, Ramesh KP, Prasad V, Shivakumara C, Chandrappa GT. Magnetoresistive studies on nanocrystalline $La_{0.8}Sr_{0.2}MnO_3$ manganite. Physica B. 2008;**403**:3360

[35] Grossin D, Noudem JG. Synthesis of fine $La_{0.8}Sr_{0.2}MnO_3$ powder by different ways. Solid State Sciences. 2004;**6**:939